Real-time Probabilistic Coupled Ocean Physics-Acoustics Forecasting and Data Assimilation for Underwater GPS

P. F. J. Lermusiaux[a,†], C. Mirabito[a], P. J. Haley, Jr.[a], W. H. Ali[a], A. Gupta[a], S. Jana[b]
E. Dorfman[c], A. Laferriere[c], A. Kofford[c], G. Shepard[c], M. Goldsmith[c],
K. Heaney[d], E. Coelho[d], J. Boyle[d], J. Murray[d], L. Freitag[e], A. Morozov[e]
[a] *Department of Mechanical Engineering, Massachusetts Institute of Technology, Cambridge, MA*
[b] *Department of Mathematics, Adamas University, Kolkata, India*
[c] *Raytheon BBN Technologies, Cambridge, MA*
[d] *OASIS, Inc., Lexington, MA*
[e] *Woods Hole Oceanographic Institute, Woods Hole, MA*
[†]Corresponding Author: pierrel@mit.edu

***Abstract*—The widely-used Global Positioning System (GPS) does not work underwater. This presents a severe limitation on the communication capabilities and deployment options for undersea assets such as AUVs and UUVs. To address this challenge, the Positioning System for Deep Ocean Navigation (POSYDON) program aims to develop an undersea system that provides omnipresent, robust positioning across ocean basins. To do so, it is critically important to accurately model sound waves and signals under diverse, and often uncertain, undersea environmental conditions. Probabilistic estimates of the four-dimensional variability of the fields of sound speed, salinity, temperature, and currents are thus needed. In this paper, we employ our MSEAS primitive-equation and error subspace data-assimilative ensemble ocean forecasting system during two real-time POSYDON sea exercises, one in winter 2017 and another in August 2018. We provide real-time high-resolution estimates of sound speed fields and their uncertainty, and describe the ocean conditions from submesoscales eddies and internal tides to warm core rings and larger-scale circulations. We verify our results against independent data of opportunity; in all cases, we show that our probabilistic forecasts demonstrate skill.**

***Index Terms*—ocean modelling, acoustic forecasting, uncertainty forecasting, data assimilation, Middle Atlantic–New York Bight**

Global Oceans 2020: Singapore - U.S. Gulf Coast | 978-1-7281-5446-6/20/$31.00 ©2020 IEEE | DOI: 10.1109/IEEECONF38699.2020.9389003

I. Introduction

The Positioning System for Deep Ocean Navigation (POSYDON) program aims to develop a Global Positioning System (GPS) for underwater assets. The primary goals of our effort are to: (1) Employ and develop our regional ocean modeling, data assimilation, and uncertainty quantification for the estimation of sound speed variability, coupled oceanographic-acoustic forecasting and inversion relevant to the Precision Ocean Interrogation, Navigation, and Timing (POINT) effort; (2) Apply our theory and schemes for optimal placement, path planning, and persistent ocean sampling with varied assets and acoustic source platforms; and (3) Further quantify the ocean dynamics and variability of the regional areas of interest, utilizing our multi-resolution data-assimilative ocean modeling and process studies.

As part of this project, we characterized the oceanographic variability and uncertainty in the Middle Atlantic Bight (MAB) region, using our MIT Multidisciplinary Simulation, Estimation, and Assimilation System (MSEAS) primitive equation (PE) modeling system [1], [2] and Error Subspace Statistical Estimation (ESSE) framework [3]–[7]. Our realistic data-assimilative modeling involved real-time ensemble forecasting and data-driven simulations and analyses of the sound speed variability. This prediction and estimation of the environmental propagating medium is uncertain because of the uncertain initial and boundary conditions, and sub-grid-scale parameterizations [8]. Just as we now utilize probabilities for rain or bad weather on a daily basis, the proposed underwater communication and global positioning system for deep ocean navigation can also utilize and benefit from such probabilistic information. Real-time integrated oceanographic-acoustic predictions must account for and forecast these uncertainties and their effects on sound propagation and communications.

This paper is organized as follows. In Sect. II, we describe our methodology and systems, and specifically our MIT-MSEAS modeling software and its setup for the real-time at-sea exercises conducted in 2017 and 2018. In Sect. III, we show and discuss our results, which include real-time forecasts of ocean physics and acoustics, as well as their uncertainty, along with validation against independent data. Finally, some concluding remarks are made and possible future research directions are discussed in Sect. IV.

II. Real-time Forecasting Setup

A. Overview

The POSYDON Sea Exercise 2017 occurred in the Middle Atlantic–New York Bight Region during January–March 2017 (Fig. 1a). Subsequently, the POSYDON Sea Exercise 2018 occurred in the same region during August 2018 (Fig. 1b). In collaboration with the POINT team, the objectives of the exercises were to utilize the MIT-MSEAS system to: (i) forecast the probability of high-resolution ocean fields using our multiscale ESSE methodology; (ii) transfer the corresponding distribution of the sound speed field to three-dimensional underwater sound propagation uncertainties; (iii) collect sufficient data to evaluate the accuracy of the Bayesian tomographic inversion and of its posterior estimates of sound velocity profiles (SVPs) and ranges between transducers.

For these exercises, we utilized and further developed our MIT-MSEAS software, including our hydrostatic PE code with a nonlinear free surface, based on second-order structured finite volumes [1], [2], [9]. The MSEAS software is used for fundamental research and for realistic simulations and predictions in varied regions of the world's ocean [10]–[20], including monitoring [21], ecosystem prediction and environmental management [22], [23], and, importantly for the present project, real-time oceanographic-acoustic predictions and coupled ocean-acoustic data assimilation [15], [24]–[28].

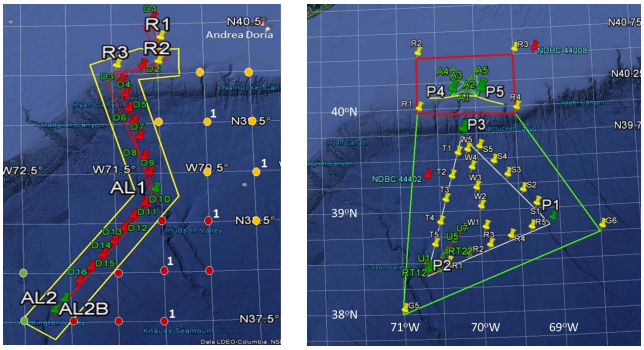

(a) 2017 configuration (b) 2018 configuration

Fig. 1. BBN mooring and (X)CTD deployment locations.

B. Probabilistic Simulations Setup

The MIT-MSEAS modeling system was set up for the computational domain shown in Fig. 2, which encompasses the northeast U.S. continental shelf, the shelfbreak and Hudson Canyon, and the northwest Sargasso Sea. It has 3 km horizontal resolution, and is discretized using 100 optimized vertical levels. The bathymetry data source is the 3 arc-second National Centers for Environmental Information (NCEI) U.S. Coastal Relief Model [29]. Tidal forcing from the TPXO8 model [30], [31] from Oregon State University is used, but updated for our high-resolution bathymetry, coastlines, and quadratic bottom drag. The probability distributions of tidal forcing fields is simulated using random variables modeling the uncertainties in key tidal parameters. Each ocean ensemble member is thus forced with slightly different tidal fields.

The 2017 ocean central forecasts are forced by atmospheric flux fields forecast by the 5 km hourly High-Resolution Window (HIRESW) from the National Centers for Environmental Prediction (NCEP), while the 2018 central forecasts are forced with flux fields from the NCEP Global Forecast System (GFS) $0.25°$ model with hourly resolution [32].

To account for uncertainties in the atmospheric forcing, for the 2017 ensemble ocean forecasts, four atmospheric forcing data sources were used: 5 km hourly NCEP High-Resolution Window (HIRESW), $0.25°$ hourly NCEP GFS, $0.5°$ 3-hourly NAVy Global Environmental Model (NAVGEM), and 6-hourly $0.15°$ Coupled Ocean/Atmosphere Mesoscale Prediction Systems (COAMPS). For the 2018 ensemble ocean forecasts, only the $0.25°$ hourly NCEP GFS was used. In all cases, forcing uncertainty was quantified using random variables

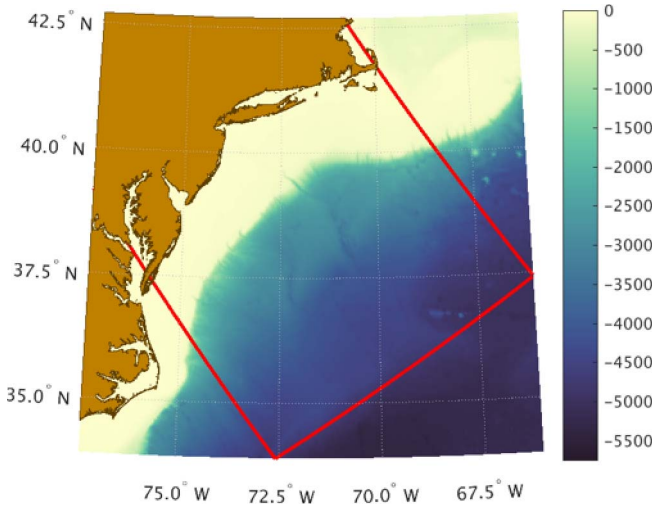

Fig. 2. MSEAS-PE 3 km modeling domain (boundary shown in red) over bathymetry (m).

(e.g. one for time-lags and one for amplitudes) such that each ocean ensemble member is forced by a different realization of atmospheric forcing fields.

In January–March 2017, atmospheric winds showed five gales (stresses at least 0.5 N/m^2) and four other strong events. During the first gale (Jan. 23), the prevailing winds were toward the southwest; during the second (Feb. 10), toward the southeast; during the third (Feb. 13–14), toward the southeast; during the fourth (Mar. 2), toward the east-northeast; during the fifth (Mar. 5), toward the southeast. In August 2018, there were three major events (stresses at least 0.25 N/m^2): during the first (Aug. 13), prevailing winds were toward the northeast; during the second (Aug. 19), toward the east-northeast; during the third (Aug. 22–23), toward the northeast.

C. Deterministic Initialization and Corrections

The ocean forecasts were initialized from 1/12° HYbrid Coordinate Ocean Model (HYCOM) analyses [33], downscaled to higher resolution and updated with ocean data from varied open sources of opportunity (CTDs, ARGO floats, gliders, SST, etc.). In addition, the following procedure was used to correct HYCOM based on our feature models, which identified two Warm Core Rings (WCR) in the region on February 20, 2017: (i) Synoptic slope water profiles with proper water masses were used to correct the initial condition slope and intrusion features; (ii) Actual synoptic profiles and copied profiles were assimilated into HYCOM; (iii) Warm Core Ring profiles were then identified and blended into the corrected HYCOM fields using sea surface temperature (SST); (iv) SST was then assimilated into the ring-corrected fields. This procedure resulted in stronger and more coherent rings (especially in the 300 m temperature field), as well as more coherent shelf and slope water between rings.

D. Ensemble Initialization and Forecasts

The Error Subspace Statistical Estimation (ESSE) probabilistic forecasts consisted of an ensemble of numerical

simulations that were each set up by perturbing the initial and boundary conditions in accord with their dominant uncertainties, and by adding stochastic forcing to the external forcing (i.e., uncertainties in the times/phases and amplitudes of the atmospheric fluxes and tides) and to the deterministic equations so as to represent modeling errors occurring during the time and space integrations of the MSEAS PE ocean modeling system [34]. In the present experiment, 100-member ensemble forecasts were issued from January 30 to February 13 and February 22 to March 6, 2017, and 300-member forecasts from August 9–24, 2018.

To initialize the uncertainties in the ocean state, we employed and further developed our data-driven initialization stochastic models [16], [24], [34]–[36]. We used historical CTD synoptic data from the World Ocean Database (WOD) from January/February for the 2017 exercise, and data from the National Marine Fisheries Service (NMFS), fishermen, gliders, Argo, and WOD from July/August for the 2018 exercise. One novelty is that we separated these data based on their regions and water masses, specifically the continental shelf, the continental slope, and the Sargasso Sea regions. These data were used to create joint vertical EOFs (empirical orthogonal functions) for temperature (T) and salinity (S), separately in each of these three regions. To construct the three-dimensional (3D) T and S perturbations in each region, the joint EOFs were combined with an eigendecomposition of a horizontal correlation matrix defined by a Mexican hat correlation function of 25 km decay-scale and 75 km zero-crossing (these numbers were obtained from the calibration PE runs and the literature). These 3D perturbations in the three regions were melded across the shelfbreak front and the Gulf Stream to form 3D perturbation fields covering the whole domain, ensuring that the melding preserved variance [37]. Finally, these 3D T and S perturbations were used to generate velocity perturbations in accordance with close-to-geostrophic PE balance.

III. Results and Discussion

A. Deterministic Forecasts

For the 2017 sea exercise, daily deterministic (central) forecasts of 2-day duration were issued for the period from January 30 to February 13, 2017, then again from February 22 to March 6, 2017. For the 2018 exercise, daily deterministic forecasts of 3-day duration were issued for the period August 9–24, 2018, as seen in the table shown in Fig. 3. For each forecast, we provide estimates of sound speed, velocity magnitude, temperature, and salinity fields every 3 hours and at 0 m, 100 m, 300 m, 500 m, and 1000 m, as well as 2 m vorticity, barotropic velocity, and surface elevation. We provide these estimates for zooms on the operational area of interest, plus those on the full modeling domain shown in Fig. 2. We also provide forecasts and analyses on three operational vertical sections defined in Fig. 4. Finally, we distribute interactive forecast visualizations [40] and specific operational products.

The MSEAS-PE relative vorticity forecast at 2 m on February 26, 2017 is shown in Fig. 5a. This forecast is a high-resolution (3 km) simulation downscaled from HYCOM. In the period leading up to February 26, submesoscale structures develop in the slope and Sargasso regions. Strong tides and the relatively well-mixed winter conditions reduce finer-scale vorticity in the shelf region. The vorticity forecast on August 26, 2018 is shown in Fig. 5b, which shows higher submesoscale structures and internal tides in the shelf region during this summer period. However, after the wind event of Aug 22-23, there are less surface submesoscale eddies in the slope and Sargasso regions than in winter.

The impact of tides on the MSEAS-PE forecasts can be seen in the deterministic forecast on February 27, 2017. During the previous few days, internal tides and internal waves are generated along the bathymetry by the tidal forcing. These waves propagate offshore. The impact of these waves can be seen in Fig. 6, which shows the sound speed cross-section between moorings R3 and AL1.

B. Deterministic Skill

Both our deterministic and ensemble forecasts were verified against independent data of opportunity. The numerous types of these data are described in Fig. 7, along with the available 2017 BBN cruise data useful for later reanalysis. The number of available profiles from a given data source on a given day is shown in Fig. 8. The profile data locations (by type) for February 18, 2017, are displayed in Fig. 9.

In Figs. 10b and 10d, we compare the temperature and salinity from the MSEAS-PE deterministic forecast for August 23, 2018 with that measured by the OOI glider GL389 (on that date, the glider is located on the shelf break). These glider profiles were not employed in the downscaled IC/BCs, nor were they assimilated; they represent independent validation data. Nevertheless, we see that the MSEAS-PE shows skill, as both the temperature and salinity profiles generally align. Quantitatively, we demonstrate in Fig. 10 that the RMSEs and biases between the simulated fields and glider profiles on Aug 23 are smaller in amplitude with the MSEAS-PE forecasts for both temperature and salinity than they are with the initial conditions (corrected HYCOM fields). Specifically, the MSEAS-PE forecast substantially reduces the RMSE profile values (on vertical average, 0.31 vs. 0.52 for T and 0.09 vs. 0.21 for S). The MSEAS-PE forecast also substantially reduces the bias profile amplitudes, for both temperature and salinity (on vertical average, 0.03 vs. 0.18 for T and insignificant values for S). This performance confirm quantitative skill: the forecasts beat persistence substantially. Similar results are obtained on other days (not shown).

We also compared our forecasts against another independent data sets, the buoy time-series from the NOAA National Data Buoy Center (NDBC) [41]. In Fig. 11, we show the comparison of the near-surface temperature data from buoy 44020 (located in Nantucket Sound; red curve) with the MSEAS-PE forecast temperature interpolated to the buoy position/depth (black curve), from August 19–23, 2018. We see that the MSEAS-PE forecast maintains skill out to 4 days, with mis-

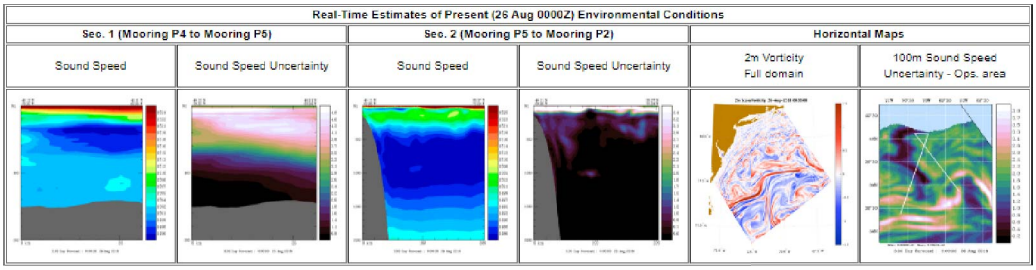

Nowcast and Forecast Products with dynamics and uncertainty descriptions			Analyses and Forecasts Issued On: August 9	10	11	12	13	14	15	16	17	18	19	19 8p	20	21	22	23	24
Ocean Physics	Horizontal Maps	Central Forecast	X	X	X	X	X	X	X	X	X	X	X	X	X	X	X	X	X
		Mean and Uncertainty	X	X	X	X	X	X	X	X	X	X	X	X	X	X	X	X	X
	Operational Vertical Sections	Central Forecast	X	X	X	X	X	X	X	X	X	X	X	X	X	X	X	X	X
		Mean and Uncertainty	X	X	X	X	X	X	X	X	X	X	X	X	X	X	X	X	X

Interactive Nowcast and Forecast Products with dynamics and uncertainty descriptions			Analyses and Forecasts Issued On: August 9	10	11	12	13	14	15	16	17	18	19	19 8p	20	21	22	23	24
Ocean Physics	Interactive Maps	Central Forecast	X	X	X	X	X	X	X	X	X	X	X	X	X	X	X	X	X
		Mean and Uncertainty	X	X	X	X	X	X	X	X	X	X	X	X	X	X	X	X	X

Fig. 3. Daily deterministic and ensemble MIT-MSEAS real-time forecasts for August 2018 [38]. The estimates of the present environmental conditions were automatically updated in real-time during the 2018 sea exercise. A similar page is available for the January–March 2017 period [39].

	2017		2018	
Section	Start	End	Start	End
1	AL2	AL1	P4	P5
2	R3	AL1	P5	P2
3	R3	R2	P4	P1

Fig. 4. BBN moorings used as the start and end points of operational vertical sections. The mooring locations are shown in Fig. 1. We provided real-time estimates of sound speed, along-section velocity, across-section velocity, temperature, and salinity in these sections, as well as their uncertainty.

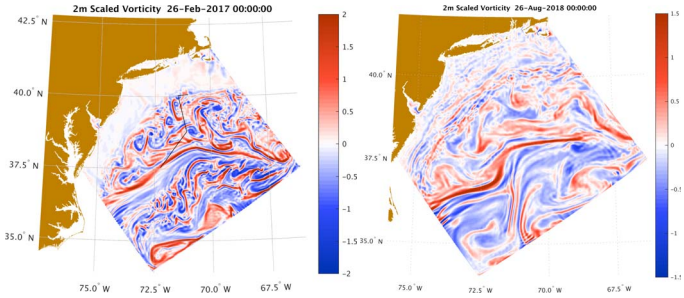

(a) February 26, 2017 (b) August 26, 2018

Fig. 5. MSEAS-PE 2 m vorticity forecasts. The location of the BBN operational vertical sections are drawn in black.

matches of less than $0.5°$C, and produces similar daily cycle excursions (both in amplitude and frequency).

Additional comparisons to ARGO, Scripps and Rutgers gliders, WHOI WaveGliders, and HF Radar data, while not shown, also indicate acceptable ocean fields forecast and real-time re-analyses.

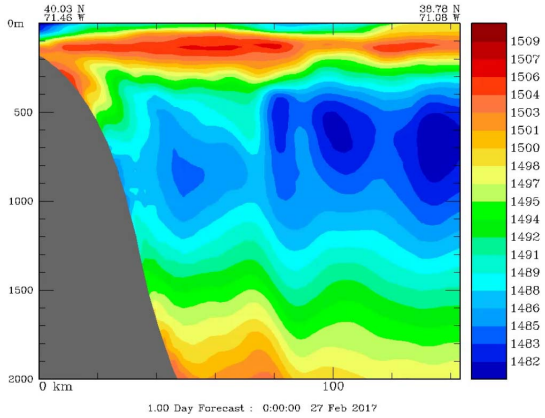

Fig. 6. MSEAS-PE sound speed cross-section between moorings R3 and AL1 on February 27, 2017. Internal tides propagate away from the shelfbreak.

C. Probabilistic Ensemble Forecasts

Using the new multi-region ESSE initialization procedure described in Sect. II-D to construct the 3D multivariate perturbations, daily ocean ensemble forecasts were issued during both the 2017 and 2018 sea exercises (for the same durations and periods as the deterministic forecasts). For each ESSE ensemble forecasts, we provide estimates every 3 hours of the ensemble mean and uncertainty (ensemble standard deviation and other statistics) of the sound speed, velocity magnitude, temperature, and salinity. Maps were provided at the same depths as the deterministic forecasts, and the same operational vertical sections were used.

To improve the quality of the forecasts, we assimilated data

Data	Variables	Duration
BBN CTD	T, S	2017-02-03 and 2017-02-18
BBN XCTD	T, S	2017-02-17 to 2017-02-24
		2017-03-06 to 2017-03-08
BBN Moorings	T, S	2017-02-19 to 2017-03-07
ALAMO Float	T	2016-10-15 to 2017-01-24
ARGO	T, S	2017-02-16 to 2017-03-30
		2018-07-02 to 2018-08-23
Current Meters	U, V	1999, 2000, 2006, 2010
GTSPP	T	2017-02-19 to 2017-03-20
HF Radar	U, V	2018-07-17 to 2018-08-31
J. Clark GS	SST	2017-02-06 to 2017-03-06
		2018-07-23 to 2018-08-13
NMFS	T, S	2017-02-11 to 2017-02-22
NOAA Buoys	T	2016-01 and 2017-01
Oleander XBT	T	2018-08-10 to 2018-08-12
OOI Gliders	T, S	2017-01-16 to 2017-04-01
		2018-07-24 to 2018-08-23
Rutgers Gliders	T, S	2018-07-05 to 2018-08-23
Satellite SST	SST	2017-02-20 and 2017-02-27
		2018-07-12 to 2018-08-24
Scripps Gliders	T, S	2018-06-20 to 2018-08-23
Sylvia Glider	T, S	2018-08-02 to 2018-08-10
WaveGlider	T, S	2018-08-09 to 2018-08-24
WOD	T, S	Jan–Feb (1974, 84, 89, 96, 99, 2006, 07, 11, 16)
		Oct–Dec (1997-8, 2014-5)

Fig. 7. Available data used as model input or validation. The BBN cruise data is listed in the upper block, while the lower block contains the data of opportunity.

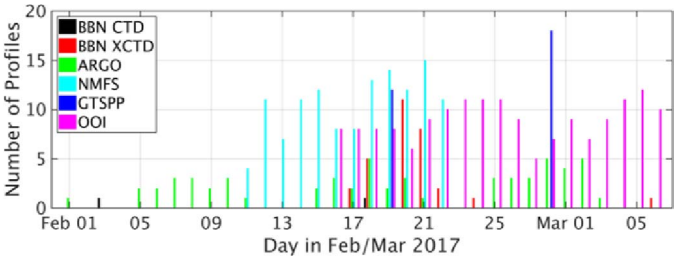

Fig. 8. Day-wise number of profiles available in February–March 2017. A much larger number of profiles are available in August 2018 because of the presence of several gliders in the modeling region.

and greatly expanded the ensemble sizes between 2017 and 2018. For the 2017 sea exercise, the daily ensemble forecasts contained 100 members, whereas for the 2018 exercise, the ensembles contained between 100 and 300 members. To facilitate collaboration, we distributed these ensemble forecasts through a novel interactive download script.

An example of our ESSE ensemble forecast for sound speed on February 21–27, 2017 along the R3-AL1 section is shown in Fig. 12. We note that assimilation of the BBN XCTD and OOI glider data reduces the initial uncertainty. Uncertainty in the warm core rings (which is advected in over time)

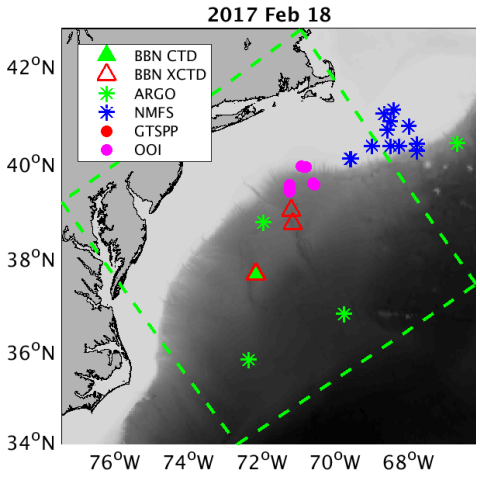

Fig. 9. Profile locations by type on February 18, 2017, overlaid on bathymetry. The MSEAS-PE domain boundary is shown in dashed green lines.

and the Gulf Stream position drives the uncertainty growth in the slope region. The probabilistic ensemble tidal forcing provides uncertainty in the position, amplitude, and phase of the internal tides and internal waves, which feeds the growth in uncertainty.

Similarly, for the 2018 exercise, the 100 m sound speed uncertainty forecast for August 26, 2018 is shown in Fig. 13. The largest standard deviation is associated with the uncertainty in the position of the Gulf Stream (south and southwest of the operational area). At that depth, sound-speed uncertainties are also larger in the slope region than in the Sargasso sea region (south of the Gulf Stream), mainly because the initial condition that reflect the historical variability.

D. Probabilistic Ensemble Forecast Skill

As with our deterministic forecasts, we verified our ensemble forecasts against independent data of opportunity. Specifically, we compared our forecasts to temperature and salinity profiles from ARGO, OOI, Rutgers, and Scripps gliders. The comparison of our 300-member ensemble with OOI glider GL389 on August 23, 2018 at 01:04Z is shown in Fig. 14. The black curves denote the forecasts for each member; the blue curve, the central forecast; the red curve, the data; and the green curve, the ensemble mean. Note that the realizations encompass the data, and the standard deviation of the ensemble is a reasonable proxy for RMSE; the data lies within the range of forecasts at all depths, and shows good agreement with the ensemble mean forecast.

Again, while the comparisons to other independent data of opportunity are not shown, they generally indicated acceptable ensemble forecast simulations.

E. Interactive Forecast Visualization

During the August 2018 sea exercise, we also provided interactive maps of our nowcast and forecast products (central forecasts as well as mean and uncertainty forecasts) using our recently developed SeaVizKit ocean visualization software [40]. SeaVizKit, built using Leaflet [42] and D3.js [43]

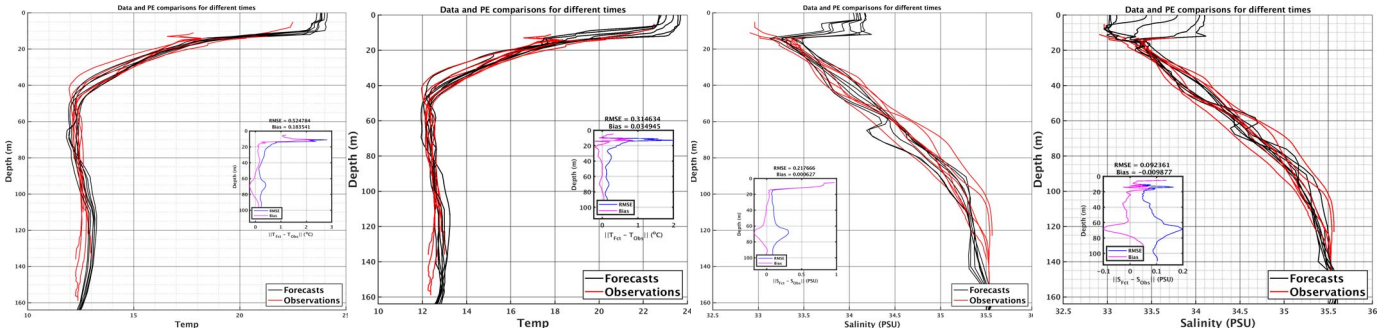

(a) Corrected HYCOM temperature (b) MSEAS-PE temperature (c) Corrected HYCOM salinity (d) MSEAS-PE salinity

Fig. 10. Deterministic forecast (black) verification against independent OOI glider GL389 data (red) on August 23, 2018. RMSE and bias profiles are plotted in the insets, along with their respective averaged values.

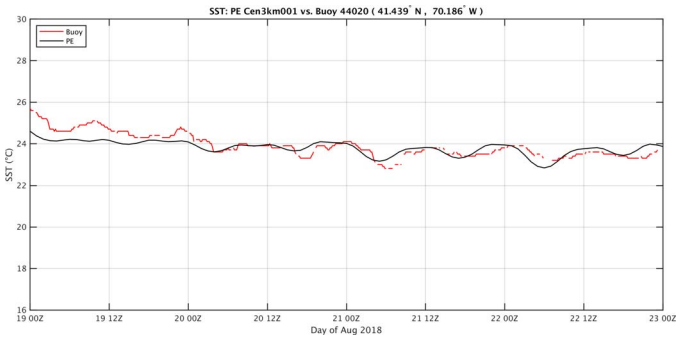

Fig. 11. MSEAS-PE deterministic forecast (black) verification against independent NDBC buoy data (red).

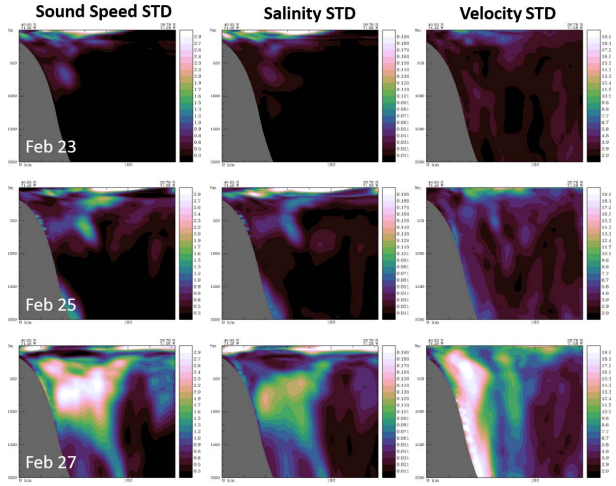

Fig. 12. Real-time ESSE ensemble forecasts of sound speed, salinity, and velocity standard deviation (uncertainty) for February 23, 25, and 27, 2017, along the R3-AL1 section.

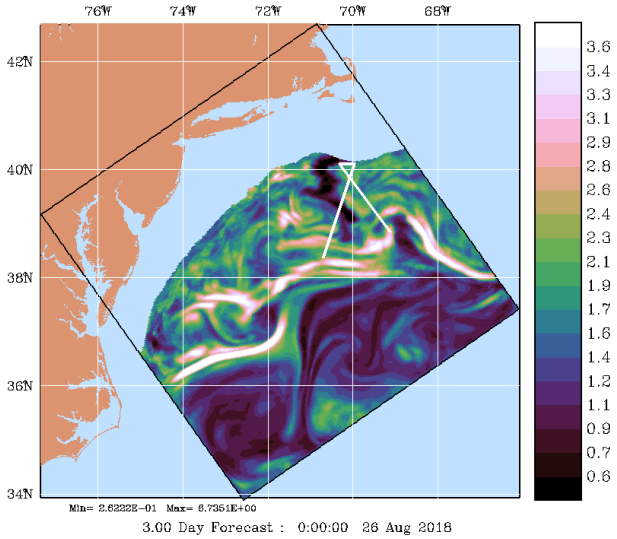

Fig. 13. Three-day real-time ESSE ensemble forecast of the standard deviation (uncertainty) of the 100 m sound speed field for August 26, 2018, as obtained by an ESSE ensemble of 300 members.

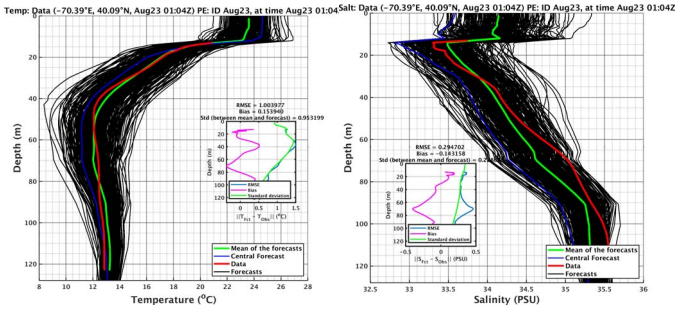

(a) Temperature (b) Salinity

Fig. 14. Real-time ESSE ensemble forecast verification against OOI glider GL389 data on August 23, 2018 at 01:04Z

JavaScript libraries, helped visualize the multivariate multi-dimensional fields forecast by the MSEAS software using a portable and highly interactive browser-based interface. Examples of such visualizations are shown in Figs. 15 and 16. Specifically, Fig. 15 shows snapshots of the surface velocity magnitude for the nowcast (a) and the forecast for August 25 18Z (b) during the 2018 sea exercise. SeaVizKit additionally overlays animated pathlines to help visualize the currents in the region. Fig. 16 shows another example application of SeaV-

izKit for visualizing the forecast of the sound speed mean (a) and uncertainty (b) fields at 100 m depth for August 25 18Z. Both examples show the interactive web interface allowing the user to pan, zoom, and switch between the several variables, depths, and times available in the forecast.

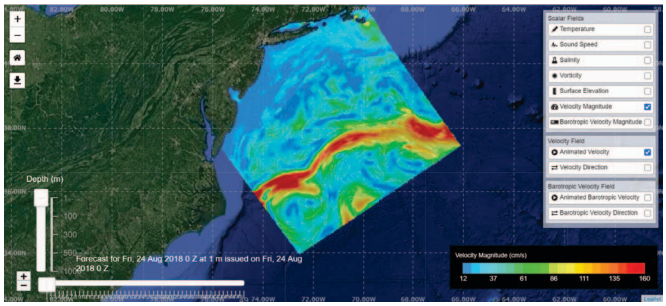

(a) Nowcast: 0Z Aug. 24, 2018

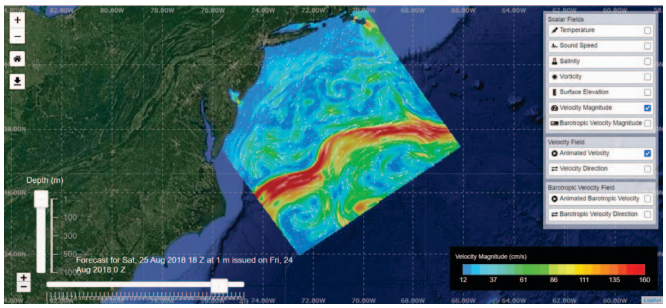

(b) Central Forecast for: 18Z Aug. 25, 2018

Fig. 15. Example SeaVizKit visualization of the surface velocity field obtained during the 2018 sea experiment. (a) Nowcast at 0Z on Aug. 24; (b) Central forecast for 18Z on Aug. 25.

F. Probabilistic Ocean Acoustics Rays

In order to perform acoustic tomography in the time domain (rather than a frequency domain matched-field approach), each ray arrival must be stable, resolvable, and identifiable. This process can be simple or complex depending upon the background ocean sound speed and the dispersion of the ray arrivals [44]. It is traditionally done painstakingly by hand.

During our real-time navigational operations, a raytrace acoustics code was run through the ensemble of ocean temperature/salinity forecasts for the expected source and receiver positions. The spread in arrival time and ray-ID was computed for each arrival, providing a look into the expected observable paths and their arrival time uncertainty. For the acoustic model, the unique ray-ID was provided by counting the number of upper and lower turning points. probabilistic rays forecasts (depth vs. arrival times) as well as the forecast arrival times (blue dots) and uncertainties for each ray ID. The data arrival with intensity level coloring is shown in the center line of colored dots. This template was used to develop an algorithm for real-time ray-identification that quantified the effects of the environmental uncertainty forecasts on the acoustic rays.

IV. Conclusions

We completed real-time sea exercises for the POSYDON-POINT project in 2017 and 2018. During each exercise, we

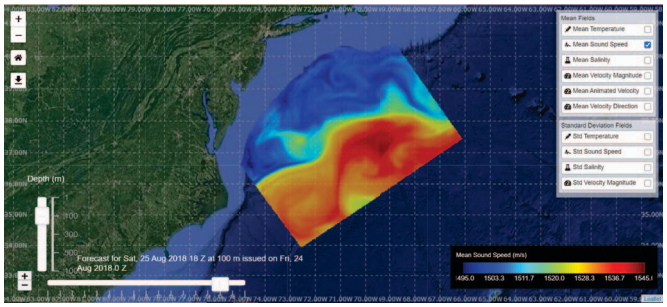

(a) Mean Forecast for: 18Z Aug. 25, 2018

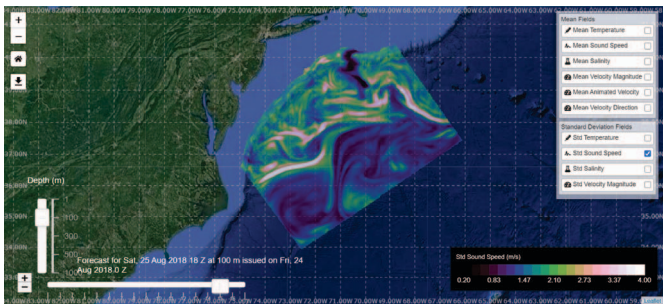

(b) Std. Dev. Forecast for: 18Z Aug. 25, 2018

Fig. 16. Example SeaVizKit visualization of the sound speed mean and uncertainty at 100 m depth obtained during the 2018 sea experiment. (a) Mean forecast at 18Z on Aug. 25; (b) Standard deviation forecast for 18Z on Aug. 25.

provided deterministic and probabilistic high-resolution forecasts using our MSEAS-PE modeling software, which includes a nonlinear free-surface, tides, and a large number of ensemble members (e.g. 300) tuned for accurate ensemble forecasting. We described our tidal and new ensemble atmospheric forcing, our multi-region multivariate 3D ensemble initialization and perturbation procedure, and our data-driven corrections to HYCOM in the shelf, slope, Sargasso regions. We verified both our central and ensemble forecasts against independent data of opportunity, and demonstrated that our model forecasts showed skill over the short-term. We expanded our visualization capabilities, allowing us to provide interactive real-time forecasts to collaborators as well as the public. Finally, our probabilistic rays forecasts including stochastic arrival times and ray IDs allowed real-time ray-identification that quantified the effects of the environmental uncertainties.

Many extensions of our present modeling results are possible. Our probabilistic forecasts are the inputs needed to forecast the reachability sets and their PDFs for gliders or floats [45]–[47], as demonstrated in a sea exercise that took place in the Arabian Sea in March–April 2017, as part of the NASCar-OPS project [16]. Higher resolution bathymetry and atmospheric forcing can be used, as well as increased data assimilation, further improving the fidelity of the forecasts. Finally, we can utilize the Dynamically-Orthogonal (DO) PE methodology to allow us to increase the ensemble size by several orders of magnitude [48], [49].

Extending the acoustic modeling capabilities is also possible. The probabilistic forecasts of the ocean environment

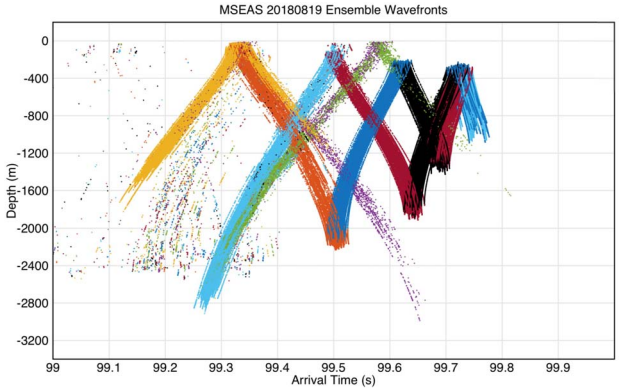

(a) Probabilistic ray depths and arrival times forecast for Aug. 19, 2018

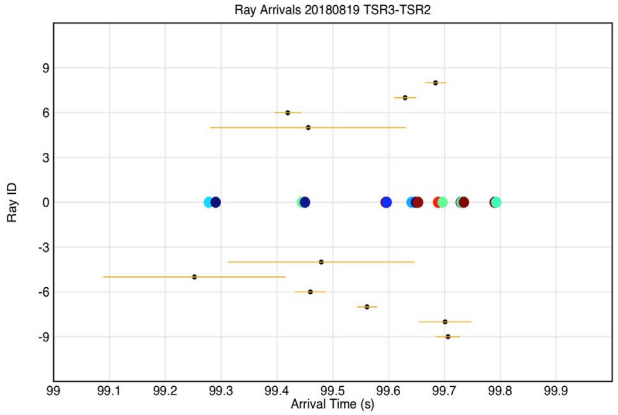

(b) Probabilistic ray IDs and arrival times forecast for Aug. 19, 2018

Fig. 17. Probabilistic ocean rays forecasts issued in real-time for Aug. 19, 2018. (a) Probabilistic rays forecasts (depth vs. arrival times) (b) Arrival times (blue dots), with uncertainties (yellow bars) for each ray ID (y-axis). The data arrival with intensity level coloring is shown in the center line of colored dots.

would allow large-ensemble probabilistic acoustic predictions using the DO methodology or other data-driven methods [50]–[52]. Such methods can then be integrated within decision aids for reliable underwater positioning, navigation and communication based on probabilistic decision theory and risk management [53]. Future work in this area may also include developing Bayesian Learning and Machine Learning (ML) tools for accurately localizing the acoustic source/receiver pairs in order to minimize the uncertainty in the surrounding environment, an utmost need for reliable underwater GPS.

ACKNOWLEDGMENTS

We thank all members of the MSEAS group, past and present. We are grateful to the Defense Advanced Research Projects Agency (DARPA) for support under grant N66001-16-C-4003 (POSYDON) and the National Science Foundation for support under grant EAR-1520825 (NSF-ALPHA) to MIT. We thank the HYCOM team for their ocean fields, NMFS (Tamara Holzwarth-Davis and Paula Fratantoni) for their survey CTD data, NCEP (Matthew Pyle, Eric Rogers, Geoff DiMego, and Arun Chawla) for their help and support for atmospheric forcing forecasts, NOAA NDBC for supplying buoy data, JHU APL for processed SST images, and CORDC for HF Radar data. We also thank the WHOI Autonomous Systems Lab (ASL) for their SDOTS WaveGlider data. Finally, we thank the OOI and the NOAA ECOA2 teams for their data.

REFERENCES

[1] P. J. Haley, Jr. and P. F. J. Lermusiaux, "Multiscale two-way embedding schemes for free-surface primitive equations in the "Multidisciplinary Simulation, Estimation and Assimilation System"," *Ocean Dynamics*, vol. 60, no. 6, pp. 1497–1537, Dec. 2010.

[2] P. J. Haley, Jr., A. Agarwal, and P. F. J. Lermusiaux, "Optimizing velocities and transports for complex coastal regions and archipelagos," *Ocean Modeling*, vol. 89, pp. 1–28, 2015.

[3] P. F. J. Lermusiaux and A. R. Robinson, "Data assimilation via Error Subspace Statistical Estimation, part I: Theory and schemes," *Monthly Weather Review*, vol. 127, no. 7, pp. 1385–1407, 1999.

[4] P. F. J. Lermusiaux, "Data assimilation via Error Subspace Statistical Estimation, part II: Mid-Atlantic Bight shelfbreak front simulations, and ESSE validation," *Monthly Weather Review*, vol. 127, no. 7, pp. 1408–1432, Jul. 1999.

[5] P. F. J. Lermusiaux, A. R. Robinson, P. J. Haley, and W. G. Leslie, "Advanced interdisciplinary data assimilation: Filtering and smoothing via error subspace statistical estimation," in *Proceedings of The OCEANS 2002 MTS/IEEE conference*. Holland Publications, 2002, pp. 795–802.

[6] P. F. J. Lermusiaux and C.-S. Chiu, "Four-dimensional data assimilation for coupled physical-acoustical fields," in *Acoustic Variability, 2002*, N. G. Pace and F. B. Jensen, Eds. Saclantcen: Kluwer Academic Press, 2002, pp. 417–424.

[7] P. F. J. Lermusiaux, J. Xu, C.-F. Chen, S. Jan, L. Chiu, and Y.-J. Yang, "Coupled ocean–acoustic prediction of transmission loss in a continental shelfbreak region: Predictive skill, uncertainty quantification, and dynamical sensitivities," *IEEE Journal of Oceanic Engineering*, vol. 35, no. 4, pp. 895–916, Oct. 2010.

[8] P. F. J. Lermusiaux, C.-S. Chiu, G. G. Gawarkiewicz, P. Abbot, A. R. Robinson, R. N. Miller, P. J. Haley, Jr, W. G. Leslie, S. J. Majumdar, A. Pang, and F. Lekien, "Quantifying uncertainties in ocean predictions," *Oceanography*, vol. 19, no. 1, pp. 92–105, 2006.

[9] MSEAS Group, "MSEAS Software," 2013. [Online]. Available: http://mseas.mit.edu/software/

[10] W. G. Leslie, A. R. Robinson, P. J. Haley, Jr, O. Logutov, P. A. Moreno, P. F. J. Lermusiaux, and E. Coelho, "Verification and training of real-time forecasting of multi-scale ocean dynamics for maritime rapid environmental assessment," *Journal of Marine Systems*, vol. 69, no. 1, pp. 3–16, 2008.

[11] R. Onken, A. Álvarez, V. Fernández, G. Vizoso, G. Basterretxea, J. Tintoré, P. Haley, Jr., and E. Nacini, "A forecast experiment in the Balearic Sea," *Journal of Marine Systems*, vol. 71, no. 1-2, pp. 79–98, 2008.

[12] P. J. Haley, Jr., P. F. J. Lermusiaux, A. R. Robinson, W. G. Leslie, O. Logoutov, G. Cossarini, X. S. Liang, P. Moreno, S. R. Ramp, J. D. Doyle, J. Bellingham, F. Chavez, and S. Johnston, "Forecasting and reanalysis in the Monterey Bay/California Current region for the Autonomous Ocean Sampling Network-II experiment," *Deep Sea Research Part II: Topical Studies in Oceanography*, vol. 56, no. 3–5, pp. 127–148, Feb. 2009.

[13] A. Gangopadhyay, P. F. Lermusiaux, L. Rosenfeld, A. R. Robinson, L. Calado, H. S. Kim, W. G. Leslie, and P. J. Haley, Jr., "The California Current system: A multiscale overview and the development of a feature-oriented regional modeling system (FORMS)," *Dynamics of Atmospheres and Oceans*, vol. 52, no. 1–2, pp. 131–169, Sep. 2011, Special issue of Dynamics of Atmospheres and Oceans in honor of Prof. A. R. Robinson.

[14] S. R. Ramp, P. F. J. Lermusiaux, I. Shulman, Y. Chao, R. E. Wolf, and F. L. Bahr, "Oceanographic and atmospheric conditions on the continental shelf north of the Monterey Bay during August 2006," *Dynamics of Atmospheres and Oceans*, vol. 52, no. 1–2, pp. 192–223, Sep. 2011, Special issue of Dynamics of Atmospheres and Oceans in honor of Prof. A. R. Robinson.

[15] M. E. G. D. Colin, T. F. Duda, L. A. te Raa, T. van Zon, P. J. Haley, Jr., P. F. J. Lermusiaux, W. G. Leslie, C. Mirabito, F. P. A. Lam, A. E. Newhall, Y.-T. Lin, and J. F. Lynch, "Time-evolving acoustic propagation modeling in a complex ocean environment," in *OCEANS - Bergen, 2013 MTS/IEEE*, 2013, pp. 1–9.

[16] P. F. J. Lermusiaux, P. J. Haley, Jr., S. Jana, A. Gupta, C. S. Kulkarni, C. Mirabito, W. H. Ali, D. N. Subramani, A. Dutt, J. Lin, A. Shcherbina, C. Lee, and A. Gangopadhyay, "Optimal planning and sampling predictions for autonomous and Lagrangian platforms and sensors in the northern Arabian Sea," *Oceanography*, vol. 30, no. 2, pp. 172–185, Jun. 2017, special issue on Autonomous and Lagrangian Platforms and Sensors (ALPS).

[17] D. N. Subramani, P. F. J. Lermusiaux, P. J. Haley, Jr., C. Mirabito, S. Jana, C. S. Kulkarni, A. Girard, D. Wickman, J. Edwards, and J. Smith, "Time-optimal path planning: Real-time sea exercises," in *Oceans '17 MTS/IEEE Conference*, Aberdeen, Jun. 2017.

[18] C. S. Kulkarni, P. J. Haley, Jr., P. F. J. Lermusiaux, A. Dutt, A. Gupta, C. Mirabito, D. N. Subramani, S. Jana, W. H. Ali, T. Peacock, C. M. Royo, A. Rzeznik, and R. Supekar, "Real-time sediment plume modeling in the Southern California Bight," in *OCEANS Conference 2018*. Charleston, SC: IEEE, Oct. 2018.

[19] A. Gupta, P. J. Haley, D. N. Subramani, and P. F. J. Lermusiaux, "Fish modeling and Bayesian learning for the Lakshadweep Islands," in *OCEANS 2019 MTS/IEEE SEATTLE*. Seattle: IEEE, Oct. 2019, pp. 1–10.

[20] P. F. J. Lermusiaux, M. Doshi, C. S. Kulkarni, A. Gupta, P. J. Haley, Jr., C. Mirabito, F. Trotta, S. J. Levang, G. R. Flierl, J. Marshall, T. Peacock, and C. Noble, "Plastic pollution in the coastal oceans: Characterization and modeling," in *OCEANS 2019 MTS/IEEE SEATTLE*. Seattle: IEEE, Oct. 2019, pp. 1–10.

[21] P. F. J. Lermusiaux, P. J. Haley, Jr, and N. K. Yilmaz, "Environmental prediction, path planning and adaptive sampling: sensing and modeling for efficient ocean monitoring, management and pollution control," *Sea Technology*, vol. 48, no. 9, pp. 35–38, 2007.

[22] Ş. T. Beşiktepe, P. F. J. Lermusiaux, and A. R. Robinson, "Coupled physical and biogeochemical data-driven simulations of Massachusetts Bay in late summer: Real-time and post-cruise data assimilation," *Journal of Marine Systems*, vol. 40–41, pp. 171–212, 2003.

[23] G. Cossarini, P. F. J. Lermusiaux, and C. Solidoro, "Lagoon of Venice ecosystem: Seasonal dynamics and environmental guidance with uncertainty analyses and error subspace data assimilation," *Journal of Geophysical Research: Oceans*, vol. 114, no. C6, Jun. 2009.

[24] P. F. J. Lermusiaux, "On the mapping of multivariate geophysical fields: Sensitivities to size, scales, and dynamics," *Journal of Atmospheric and Oceanic Technology*, vol. 19, no. 10, pp. 1602–1637, 2002.

[25] A. R. Robinson and P. F. J. Lermusiaux, "Prediction systems with data assimilation for coupled ocean science and ocean acoustics," in *Proceedings of the Sixth International Conference on Theoretical and Computational Acoustics*, A. Tolstoy et al, Ed. World Scientific Publishing, 2004, pp. 325–342, refereed invited Keynote Manuscript.

[26] J. Xu, P. F. J. Lermusiaux, P. J. Haley Jr., W. G. Leslie, and O. G. Logutov, "Spatial and Temporal Variations in Acoustic propagation during the PLUSNet-07 Exercise in Dabob Bay," in *Proceedings of Meetings on Acoustics (POMA)*, vol. 4. Acoustical Society of America 155th Meeting, 2008, p. 11.

[27] F.-P. A. Lam, P. J. Haley, Jr., J. Janmaat, P. F. J. Lermusiaux, W. G. Leslie, M. W. Schouten, L. A. te Raa, and M. Rixen, "At-sea real-time coupled four-dimensional oceanographic and acoustic forecasts during Battlespace Preparation 2007," *Journal of Marine Systems*, vol. 78, no. Supplement, pp. S306–S320, Nov. 2009.

[28] T. F. Duda, Y.-T. Lin, W. Zhang, B. D. Cornuelle, and P. F. J. Lermusiaux, "Computational studies of three-dimensional ocean sound fields in areas of complex seafloor topography and active ocean dynamics," in *Proceedings of the 10th International Conference on Theoretical and Computational Acoustics*, Taipei, Taiwan, 2011.

[29] National Centers for Environmental Information (NCEI), "Coastal Relief Model," Aug. 2018. [Online]. Available: https://www.ngdc.noaa.gov/mgg/coastal/crm.html

[30] G. D. Egbert and S. Y. Erofeeva, "Efficient inverse modeling of barotropic ocean tides," *Journal of Atmospheric and Oceanic Technology*, vol. 19, no. 2, pp. 183–204, 2002.

[31] ——, "TPXO8-ATLAS," 2013, oregon State University. [Online]. Available: https://www.tpxo.net/global/tpxo8-atlas

[32] National Centers for Environmental Prediction (NCEP), "Global Forecast System," 2018. [Online]. Available: https://www.nco.ncep.noaa.gov/pmb/products/gfs/

[33] J. A. Cummings and O. M. Smedstad, "Variational data assimilation for the global ocean," in *Data Assimilation for Atmospheric, Oceanic and Hydrologic Applications*, S. K. Park and L. Xu, Eds. Berlin, Heidelberg: Springer Berlin Heidelberg, 2013, vol. II, pp. 303–343.

[34] P. F. J. Lermusiaux, "Uncertainty estimation and prediction for interdisciplinary ocean dynamics," *Journal of Computational Physics*, vol. 217, no. 1, pp. 176–199, 2006.

[35] P. F. J. Lermusiaux, D. G. M. Anderson, and C. J. Lozano, "On the mapping of multivariate geophysical fields: Error and variability subspace estimates," *Quarterly Journal of the Royal Meteorological Society*, vol. 126, no. 565, pp. 1387–1429, 2000.

[36] P. F. J. Lermusiaux, "Adaptive modeling, adaptive data assimilation and adaptive sampling," *Physica D: Nonlinear Phenomena*, vol. 230, no. 1, pp. 172–196, 2007.

[37] P. F. J. Lermusiaux and P. J. H. Jr., "Mseas report on stochastic forcing for pe models," Department of Mechanical Engineering, Massachusetts Institute of Technology, Cambridge, MA, USA, MSEAS Report 29, 2014.

[38] MSEAS Group, "BBN POSYDON Sea Ex 18," Aug. 2018. [Online]. Available: http://mseas.mit.edu/Sea_exercises/POSYDON-POINT/2018/

[39] ——, "BBN POSYDON Sea Ex 17," Mar. 2017. [Online]. Available: http://mseas.mit.edu/Sea_exercises/POSYDON-POINT/

[40] W. H. Ali, M. H. Mirhi, A. Gupta, C. S. Kulkarni, C. Foucart, M. M. Doshi, D. N. Subramani, C. Mirabito, P. J. Haley, Jr., and P. F. J. Lermusiaux, "Seavizkit: Interactive maps for ocean visualization," in *OCEANS 2019 MTS/IEEE SEATTLE*. Seattle: IEEE, Oct. 2019, pp. 1–10.

[41] National Oceanic and Atmospheric Administration (NOAA), "National Data Buoy Center (NDBC)," Aug. 2018. [Online]. Available: https://www.ndbc.noaa.gov/

[42] P. Crickard III, *Leaflet. js essentials*. Packt Publishing Ltd, 2014.

[43] N. Q. Zhu, *Data visualization with D3. js cookbook*. Packt Publishing Ltd, 2013.

[44] W. Munk, P. Worcester, and C. Wunsch, *Ocean acoustic tomography*. Cambridge university press, 2009.

[45] P. F. J. Lermusiaux, D. N. Subramani, J. Lin, C. S. Kulkarni, A. Gupta, A. Dutt, T. Lolla, P. J. Haley, Jr., W. H. Ali, C. Mirabito, and S. Jana, "A future for intelligent autonomous ocean observing systems," *Journal of Marine Research*, vol. 75, no. 6, pp. 765–813, Nov. 2017, the Sea. Volume 17, The Science of Ocean Prediction, Part 2.

[46] D. N. Subramani, Q. J. Wei, and P. F. J. Lermusiaux, "Stochastic time-optimal path-planning in uncertain, strong, and dynamic flows," *Computer Methods in Applied Mechanics and Engineering*, vol. 333, pp. 218–237, 2018.

[47] C. S. Kulkarni and P. F. J. Lermusiaux, "Three-dimensional time-optimal path planning in the ocean," *Ocean Modelling*, vol. 152, Aug. 2020.

[48] F. Feppon and P. F. J. Lermusiaux, "Dynamically orthogonal numerical schemes for efficient stochastic advection and Lagrangian transport," *SIAM Review*, vol. 60, no. 3, pp. 595–625, 2018.

[49] D. N. Subramani, "Probabilistic regional ocean predictions: Stochastic fields and optimal planning," Ph.D. dissertation, Massachusetts Institute of Technology, Department of Mechanical Engineering, Cambridge, Massachusetts, Feb. 2018.

[50] W. H. Ali, M. S. Bhabra, P. F. J. Lermusiaux, A. March, J. R. Edwards, K. Rimpau, and P. Ryu, "Stochastic oceanographic-acoustic prediction and Bayesian inversion for wide area ocean floor mapping," in *OCEANS 2019 MTS/IEEE SEATTLE*. Seattle: IEEE, Oct. 2019, pp. 1–10.

[51] T. F. Duda, Y.-T. Lin, A. E. Newhall, K. R. Helfrich, J. F. Lynch, W. G. Zhang, P. F. J. Lermusiaux, and J. Wilkin, "Multiscale multiphysics data-informed modeling for three-dimensional ocean acoustic simulation and prediction," *Journal of the Acoustical Society of America*, vol. 146, no. 3, pp. 1996–2015, Sep. 2019.

[52] P. F. J. Lermusiaux, P. J. Haley, Jr., C. Mirabito, W. H. Ali, M. Bhabra, P. Abbot, C.-S. Chiu, and C. Emerson, "Multi-resolution probabilistic ocean physics-acoustic modeling: Validation in the New Jersey continental shelf," in *OCEANS 2020 IEEE/MTS*. IEEE, Oct. 2020, in press.

[53] D. N. Subramani and P. F. J. Lermusiaux, "Risk-optimal path planning in stochastic dynamic environments," *Computer Methods in Applied Mechanics and Engineering*, vol. 353, pp. 391–415, Aug. 2019.